Eur. Phys. J. C 47, 171–186 (2006)
Digital Object Identifier (DOI) 10.1140/epjc/s2006-02530-x

THE EUROPEAN PHYSICAL JOURNAL C

Phenomenological analysis connecting proton–proton and antiproton–proton elastic scattering

R.F. Ávila[1], S.D. Campos[2], M.J. Menon[2,a], J. Montanha[2]

[1] Instituto de Matemática, Estatística e Computação Científica, Universidade Estadual de Campinas, 13083-970 Campinas, SP Brazil
[2] Instituto de Física Gleb Wataghin Universidade Estadual de Campinas, 13083-970 Campinas, SP Brazil

Received: 23 November 2005 / Revised version: 9 February 2006 /
Published online: 19 April 2006 –

Abstract. Based on the behavior of the elastic scattering data, we introduce an almost model-independent parameterization for the imaginary part of the scattering amplitude, with the energy and momentum transfer dependences inferred on an empirical basis and selected by rigorous theorems and bounds from axiomatic quantum field theory. The corresponding real part is analytically evaluated by means of dispersion relations, allowing connections between particle–particle and particle–antiparticle scattering. Simultaneous fits to proton–proton and antiproton–proton experimental data in the forward direction and also including data beyond the forward direction lead to a predictive formalism in both energy and momentum transfer. We compare our extrapolations with predictions from some popular models and discuss the applicability of the results in the normalization of elastic rates that can be extracted from present and future accelerator experiments (Tevatron, RHIC and LHC).

PACS. 13.85.Dz; 13.85.-t

1 Introduction

Elastic hadron–hadron scattering, the simplest hadronic collision process, still remains one of the topical theoretical problems in particle physics at high energies. In the absence of a pure QCD description of these large-distance scattering states (soft diffraction), an empirical analysis based on model-independent fits to the physical quantities involved plays an important role in the extraction of novel information, that can contribute with the development of useful calculational schemes in the underlying field theory.

In this context, empirical parameterizations of the scattering amplitude and fits to the differential cross section data have widely been used as a source of the model-independent determination of several quantities of interest (the inverse problem), such as the profile, the eikonal, the inelastic overlap functions, and, with some additional hypotheses, even information on the form factors (momentum transfer space). These aspects were recently reviewed and discussed in [1], where a list of references to some essential results can also be found. However, one aspect of this kind of analysis concerns its local description of the experimental data; that is, the free parameters are inferred from fits to each energy and to each interaction process, and therefore the approach has no predictive character. In this work we present a novel parameterization for the imaginary part of the elastic scattering amplitude with energy and momentum dependences extracted from the empirical behavior of the experimental data and selected according to some high-energy theorems and bounds from axiomatic quantum field theory. The real part of the amplitude is analytically evaluated by means of dispersion relations, connecting, therefore, particle–particle and particle–antiparticle scattering. In this context, the scattering amplitude is expressed as entire functions of the momentum transfer and of the logarithm of the energy. Global fits to proton–proton (pp) and antiproton–proton ($\bar{p}p$) experimental data in the forward direction (total cross section and the ρ parameter) and, in a second step, also including the differential cross sections, lead to a predictive formalism in the energy and momentum transfer, which is also essentially model independent. We present extrapolations for values of the energy and momentum transfer above those reached in experiments and compare with predictions from some phenomenological models. We also discuss the applicability of the results in the normalization of the elastic rates that can be measured in present and future accelerator experiments (Fermilab Tevatron, Brookhaven RHIC and CERN LHC).

As will be stressed, this analysis must be seen as a first step or attempt toward a formally rigorous model-independent description of high-energy elastic hadron

[a] e-mail: menon@ifi.unicamp.br

scattering, embodying a predictive character. In this sense we shall attempt to discuss and explain, in certain detail, the advantages and disadvantages of the present analysis and results.

The paper is organized as follows. In Sect. 2 we discuss the empirical and formal bases of the parameterization for the imaginary part of the scattering amplitude and the analytical determination of the corresponding real part by means of dispersion relations. In Sect. 3 we present the fit procedures and results, treating firstly only the forward scattering and, in a second step, including the differential cross section data. In Sect. 4 we discuss the physical implications and applicability of the approach, in the experimental and phenomenological contexts. The conclusions and some final remarks are the contents of Sect. 5.

2 Analytical parameterization for the scattering amplitude

The physical quantities that characterize the elastic hadron scattering are given in terms of the scattering amplitude F, which is expressed as a function of two Mandelstam variables in the center-of-mass system, usually the energy squared s and the momentum transfer squared $t = -q^2$. We shall base our discussion on the following physical quantities [2]: the differential cross section,

$$\frac{\mathrm{d}\sigma}{\mathrm{d}q^2} = \frac{1}{16\pi s^2}|\mathrm{Re}\,F(s,q^2) + \mathrm{i}\,\mathrm{Im}\,F(s,q^2)|^2 \ , \qquad (1)$$

the total cross section (optical theorem),

$$\sigma_{\mathrm{tot}}(s) = \frac{\mathrm{Im}\,F(s,q^2=0)}{s} \ , \qquad (2)$$

the ρ parameter (related with the phase of the amplitude in the forward direction),

$$\rho(s) = \frac{\mathrm{Re}\,F(s,q^2=0)}{\mathrm{Im}\,F(s,q^2=0)} \ , \qquad (3)$$

and the slope of the differential cross section in the forward direction,

$$B(s) = \frac{\mathrm{d}}{\mathrm{d}q^2}\left[\ln\frac{\mathrm{d}\sigma}{\mathrm{d}q^2}(s,q^2)\right]_{q^2=0} \ . \qquad (4)$$

Equations (1) and (2) represent normalizations valid in the high-energy region, for example $\sqrt{s} > 20\,\mathrm{GeV}$ [2]. We shall return to this point in what follows. In this section we first discuss in certain detail the empirical and formal bases that lead to an almost model-independent analytical parameterization for the imaginary part of the amplitude in terms of both energy and momentum transfer variables. We then treat the analytical evaluation of the corresponding real part by means of derivative dispersion relations and the analytical connections between pp and $\bar{p}p$ scattering.

2.1 Parameterization for the imaginary part of the amplitude

2.1.1 Empirical bases

Let us first investigate some empirical information on the differential cross section, in the region of small momentum transfer, $q^2 \leq 0.2\,\mathrm{GeV}^2$. In particular, it is known that, at $q^2 = 0$, the data indicate that $|\rho(s)| \leq 0.15$, as illustrated in Fig. 1. Therefore, it is expected that, at small values of the momentum transfer, the amplitude $F(s,q^2)$ is to be dominantly imaginary, so that the differential cross section in this region can be expressed as

$$\frac{\mathrm{d}\sigma}{\mathrm{d}q^2} \approx \frac{1}{16\pi}\left[\frac{\mathrm{Im}\,F(s,q^2)}{s}\right]^2 \ .$$

Moreover, in this region, the differential cross section data are approximately linear on a logarithm scale, as exemplified in Fig. 2, which means that we can express the imaginary part of the amplitude by

$$\frac{\mathrm{Im}\,F(s,q^2)}{s} \approx \alpha \mathrm{e}^{-\beta q^2} \ ,$$

where α and β are real parameters that can depend on the energy and reaction considered.

The point now is to look for possible empirical dependences for these parameters in terms of the energy s, namely analytical expressions for $\alpha(s)$ and $\beta(s)$, and that is one of the novel aspects of this work. From the above two equations and from (2) and (4) we have that $\alpha(s) \propto \sigma_{\mathrm{tot}}(s)$ and $\beta(s) \propto B(s)$. On the other hand, the empirical behavior of $\sigma_{\mathrm{tot}}(s)$ and $B(s)$ (near the forward direction), displayed in Figs. 3 and 4, respectively, indicates that in the region of high energies the empirical trends of the data (above $\sqrt{s} \approx 20\,\mathrm{GeV}$) follow polynomial dependences in $\ln s$, of second degree (total cross section) and first degree (slope). For these reasons it is reasonable to introduce the following empirical parameterizations for $\alpha(s)$ and $\beta(s)$:

$$\alpha(s) = A + B\,\ln s + C\,\ln^2 s \ ,$$

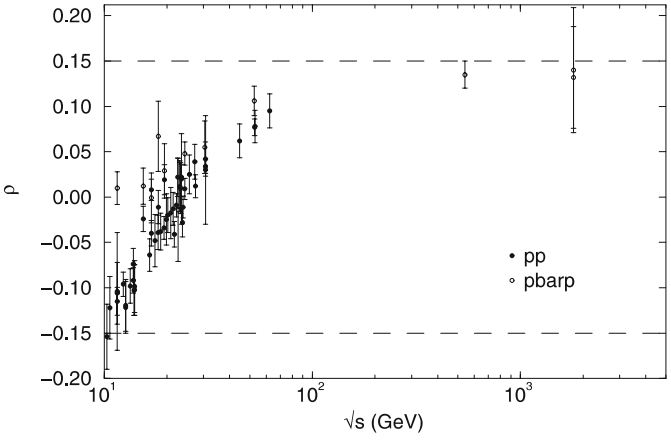

Fig. 1. Dependence of ρ from pp and $\bar{p}p$ elastic scattering (data from [3, 4])

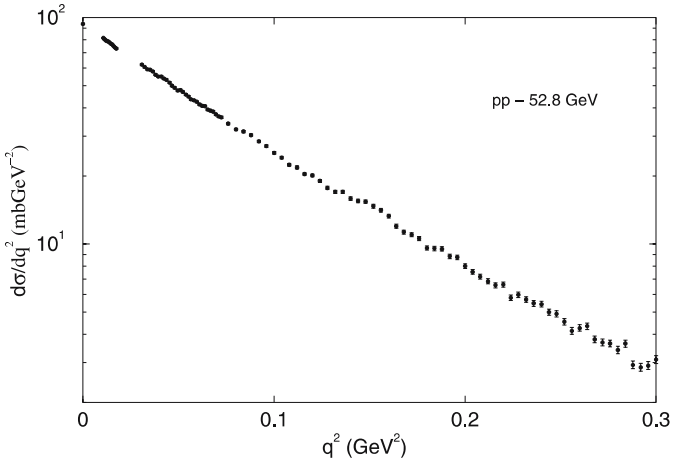

Fig. 2. Diffraction peak from pp elastic scattering at $\sqrt{s} = 52.8$ GeV [5]

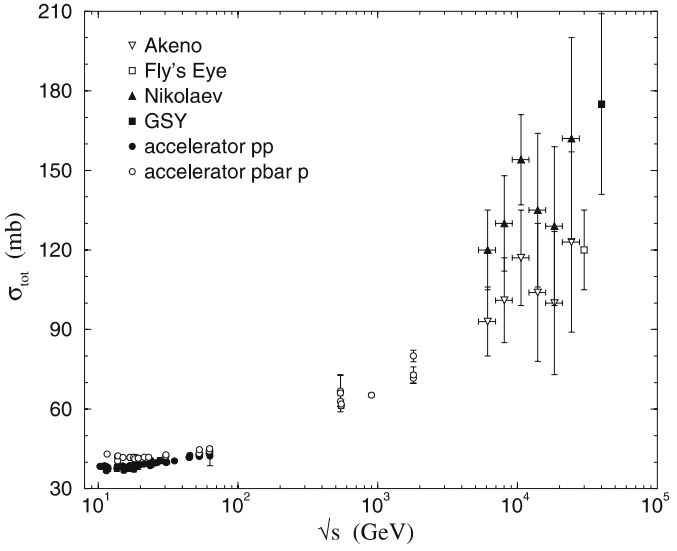

Fig. 3. Experimental information on the pp and $\bar{p}p$ total cross sections from accelerator [3] and cosmic-ray experiments (see [6] for a complete list of references and discussions)

and

$$\beta(s) = D + E \ln s \ ,$$

where A, B, C, D and E are real constants. We note that a dimensionally necessary factor s_0, in $\ln s/s_0$, is automatically absorbed by the other constants. We also note that the choice for $\alpha(s)$ is in agreement with the universal asymptotic behavior of the total cross sections from the analysis developed by the COMPETE Collaboration [9].

Now, in the region of medium and large momentum transfer, the differential cross section data is characterized by the diffractive pattern, as illustrated in Fig. 5. Since we have a logarithmic scale, this behavior can be taken into account by the standard sum of exponentials in q^2.

From the above discussion and aimed to treat both pp and $\bar{p}p$ elastic scattering, we introduce the following empirical parameterizations for pp scattering:

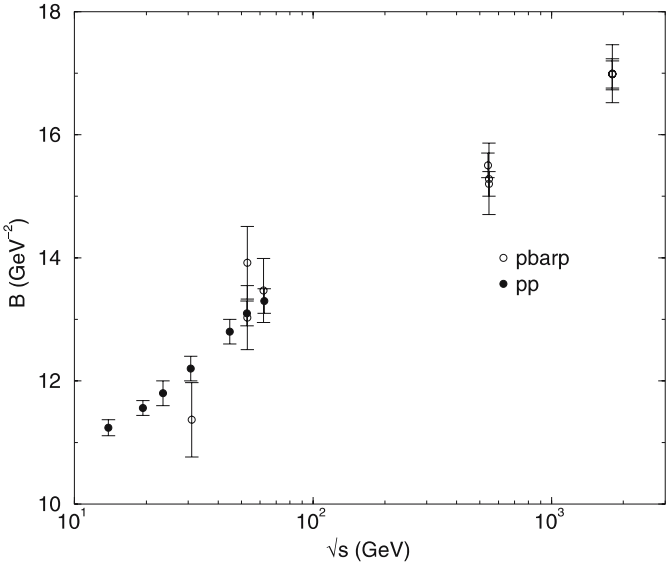

Fig. 4. The slope parameter as function of the energy and determined in the interval $0.01 < q^2 < 0.20\ \mathrm{GeV}^2$ [7, 8]

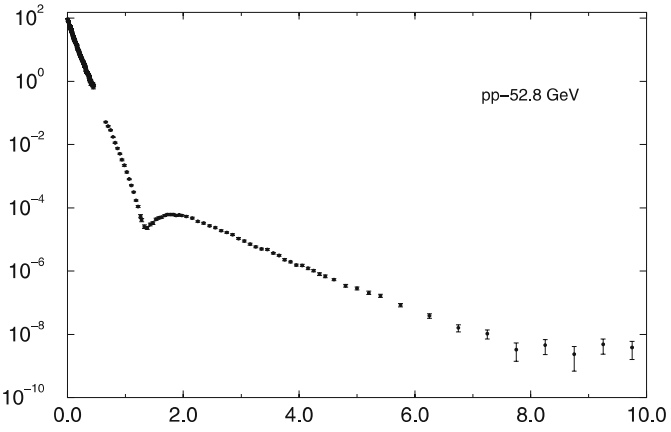

Fig. 5. Proton–proton differential cross section data at $\sqrt{s} = 52.8$ GeV [5]

$$\frac{\mathrm{Im}F_{pp}(s,q^2)}{s} = \sum_{i=1}^{n} \alpha_i(s) \mathrm{e}^{-\beta_i(s)q^2} \ , \tag{5}$$

with

$$\begin{aligned} \alpha_i(s) &= A_i + B_i \ln(s) + C_i \ln^2(s) \ , \\ \beta_i(s) &= D_i + E_i \ln(s) \ , \end{aligned} \tag{6}$$

and for $\bar{p}p$ scattering:

$$\frac{\mathrm{Im}F_{\bar{p}p}(s,q^2)}{s} = \sum_{i=1}^{n} \bar{\alpha}_i(s) \mathrm{e}^{-\bar{\beta}_i(s)q^2} \ , \tag{7}$$

with

$$\begin{aligned} \bar{\alpha}_i(s) &= \bar{A}_i + \bar{B}_i \ln(s) + \bar{C}_i \ln^2(s) \ , \\ \bar{\beta}_i(s) &= \bar{D}_i + \bar{E}_i \ln(s) \ , \end{aligned} \tag{8}$$

where $i = 1, 2, \ldots, n$. In what follows we shall check these parameterizations in a formal context.

2.1.2 Constraints from axiomatic quantum field theory

Even after QCD, unitarity, analyticity, crossing and their connections with axiomatic quantum field theory (AQFT) still remain a fundamental theoretical framework in the investigation of high-energy soft scattering. In this context, important high-energy theorems and bounds have been demonstrated [10–13], providing rigorous formal constraints in the region of asymptotic energies, which cannot be disregarded in any reliable formalism, mainly related with model-independent approaches. Since the parameterization equations (5)–(8) were based exclusively on the behavior of the experimental data at fixed (finite) energies, it is necessary to check the most important formal asymptotic results.

Firstly we note that from the optical theorem (2), the parameterizations for $\alpha_i(s)$ and $\bar{\alpha}_i(s)$ do not violate the Froissart–Martin bound, a rigorous prediction of quantum field theory [14] which states that

$$\sigma_{\rm tot} \leq c \ln^2 s \ ,$$

where c is a constant.

Another important result concerns the behavior of the difference between particle–particle and antiparticle–particle cross sections at the asymptotic regime. In this context it has been demonstrated by Eden [10] and by Grunberg and Truong [15] that if the Froissart–Martin bound is reached, the difference between the pp and $\bar{p}p$ total cross sections goes as

$$\Delta\sigma = \sigma_{\rm tot}^{pp} - \sigma_{\rm tot}^{\bar{p}p} \leq c \frac{\sigma_{\rm tot}^{pp} + \sigma_{\rm tot}^{\bar{p}p}}{\ln s} \ ,$$

which means that the difference can increases at most as $\ln s$ and even in this case,

$$\frac{\sigma_{\rm tot}^{\bar{p}p}}{\sigma_{\rm tot}^{pp}} \to 1 \ ,$$

as $s \to \infty$ (the generalized or revised form of the Pomeranchuk theorem).

Now, from the optical theorem, (2) and the parameterizations (5)–(8) we have

$$\Delta\sigma = \sum_{i=1}^{n} \left\{ (A_i - \bar{A}_i) + (B_i - \bar{B}_i) \ln s + (C_i - \bar{C}_i) \ln^2 s \right\} ,$$

and therefore, in order to not violate the above formal results, we must impose the constraint

$$\sum_{i=1}^{n} (C_i - \bar{C}_i) = 0 \ . \tag{9}$$

With this condition we also ensure another important formal result, namely that if the Froissart–Martin bound is reached the ρ parameter must go to zero logarithmically [16]

$$\rho(s \to \infty) \propto \frac{1}{\ln s} \ .$$

With the parameterizations (5)–(8) and the constraint (9) we have $10n - 1$ free parameters, where n is the number of exponentials. The novelty in these parameterizations is the fact that the energy dependences are already enclosed and were inferred from the empirical behavior of the experimental data, being also in agreement with the above high-energy theorems. Moreover, the imaginary parts of the amplitudes are entire functions of the logarithm of the energy, which is an important property in the evaluation of the real part, as discussed in what follows.

2.2 Analytical evaluation of the real part of the amplitude

Connections between real and imaginary parts of the forward scattering amplitude have been widely investigated by means of dispersion relations in both integral and derivative forms. In this work we make use of the derivative relations [17, 18], which are valid in the forward direction and for amplitudes belonging to a sub-class of entire functions of the logarithm of the energy, as is the case here. For a recent review and critical analysis on the replacement of integral relations by derivative ones see [19], where a list of references to some outstanding works can also be found.

In the forward direction, the derivative dispersion relations for even (+) and odd (−) amplitudes are expressed in terms of a tangent operator and in the case of one subtraction (equal to two subtractions in the even case) they are given by [17–19]

$$\frac{\mathrm{Re}\, F_+(s)}{s} = \frac{K}{s} + \tan\left[\frac{\pi}{2} \frac{\mathrm{d}}{\mathrm{d}\ln s}\right] \frac{\mathrm{Im}\, F_+(s)}{s} \ , \tag{10}$$

$$\frac{\mathrm{Re}\, F_-(s)}{s} = \tan\left[\frac{\pi}{2} \left(1 + \frac{\mathrm{d}}{\mathrm{d}\ln s}\right)\right] \frac{\mathrm{Im}\, F_-(s)}{s} \ , \tag{11}$$

where K is the subtraction constant. It has also been demonstrated by Fischer and Kolář [20] that at high energies the above tangent operator can be replaced by its first order expansion, which is the case we are interested in.

Since besides the forward data we also aim to investigate differential cross sections, it is necessary to consider the applicability of the dispersion techniques beyond the forward direction. Although several authors make use of dispersion relations even for large values of the momentum transfer, it is important to recall that what is formally expected is the validity of the dispersion relations, with a finite number of subtractions, inside a region $q^2 \leq q^2_{\rm max}$. However, the exact expression and/or numerical value of $q^2_{\rm max}$ depends on the theoretical framework and scattering process considered. We shall discuss this subject in some detail in Sect. 3.2.2, when applying the formalism to the experimental data. Here we only consider a reference to this limited interval.

Based on the above arguments we shall make use of the first order derivative dispersion relations, also extended beyond the forward region, namely $0 \le q^2 \le q^2_{\max}$, in the form

$$\frac{\mathrm{Re}\, F_+(s,q^2)}{s} = \frac{K}{s} + \frac{\pi}{2}\frac{\mathrm{d}}{\mathrm{d}\ln s}\frac{\mathrm{Im}\, F_+(s,q^2)}{s}\,, \qquad (12)$$

$$\frac{\mathrm{Re}\, F_-(s,q^2)}{s} = \frac{\pi}{2}\left(1+\frac{\mathrm{d}}{\mathrm{d}\ln s}\right)\frac{\mathrm{Im}\, F_-(s,q^2)}{s}\,. \qquad (13)$$

Finally, the connections between the hadronic and the even/odd amplitudes is established through the usual definitions:

$$\begin{aligned} F_{pp}(s,q^2) &= F_+(s,q^2) + F_-(s,q^2),\\ F_{\bar{p}p}(s,q^2) &= F_+(s,q^2) - F_-(s,q^2). \end{aligned} \qquad (14)$$

This approach is characterized by analytical results for both real and imaginary parts of the pp and $\bar{p}p$ amplitudes. Schematically, from the parameterizations (5)–(8) for $\mathrm{Im}\, F_{pp/\bar{p}p}(s,q^2)/s$ we obtain $\mathrm{Im}\, F_{+/-}(s,q^2)/s$ by inverting (14). Then the derivative relations (12)–(13) allow one to evaluate $\mathrm{Re}\, F_{+/-}(s,q^2)/s$ and by (14) we obtain the hadronic real parts

$$\begin{aligned} \frac{\mathrm{Re}\, F_{pp}(s,q^2)}{s} &= \frac{K}{s}\\ &+ \sum_{i=1}^{n}\left\{\frac{\pi}{2}\left[\alpha_i'(s) - \alpha_i(s)\beta_i'(s)q^2\right]\mathrm{e}^{-\beta_i(s)q^2}\right.\\ &\left. + \frac{\pi}{4}\left[\alpha_i(s)\mathrm{e}^{-\beta_i(s)q^2} - \bar{\alpha}_i(s)\mathrm{e}^{-\bar{\beta}_i(s)q^2}\right]\right\},\\ \frac{\mathrm{Re}\, F_{\bar{p}p}(s,q^2)}{s} &= \frac{K}{s}\\ &+ \sum_{i=1}^{n}\left\{\frac{\pi}{2}\left[\bar{\alpha}_i'(s) - \bar{\alpha}_i(s)\bar{\beta}_i'(s)q^2\right]\mathrm{e}^{-\bar{\beta}_i(s)q^2}\right.\\ &\left. - \frac{\pi}{4}\left[\alpha_i(s)\mathrm{e}^{-\beta_i(s)q^2} - \bar{\alpha}_i(s)\mathrm{e}^{-\bar{\beta}_i(s)q^2}\right]\right\}, \end{aligned}$$

where the primes denote differentiation with respect to $\ln s$; see (6) and (8). With this we have analytical expressions for the pp and $\bar{p}p$ differential cross sections:

$$\frac{\mathrm{d}\sigma_{pp/\bar{p}p}}{\mathrm{d}q^2} = \frac{1}{16\pi}\left|\frac{\mathrm{Re}\, F_{pp/\bar{p}p}(s,q^2)}{s} + \mathrm{i}\frac{\mathrm{Im}\, F_{pp/\bar{p}p}(s,q^2)}{s}\right|^2 .$$

It should be noted that exact analyticity and crossing properties demand symmetric variables, namely the laboratory energy E for $q^2 = 0$ and the variable $(s-u)/4m$, where u is the Mandelstam variable, for $q^2 > 0$ [2]. However, since E depends linearly on s and, as will be discussed in Sect. 3.2, we shall consider the applicability of the formalism mainly in limited regions of the momentum transfer and only above $\sqrt{s} = 20\,\mathrm{GeV}$, the use of s as variable does not introduce essential changes in the above formulas.

Taking into account the subtraction constant K, the constraint (9) and the parameterizations (5)–(8) we eventually have $10n$ fit parameters in the case of n exponential terms. This completes the analytical construction of the formalism, characterized by its empirical basis, the essentially model-independent parameterizations, the agreement with high-energy theorems and the amplitudes belonging to the class of entire functions in the logarithm of the energy. In the next section we determine the free parameters involved through fits to the pp and $\bar{p}p$ elastic scattering data.

3 Experimental data, fitting and results

3.1 Experimental data

The most important empirical input in our parameterization is the energy dependence enclosed in the expressions of $\alpha(s)$ and $\beta(s)$, (6) and (8), respectively. Since it characterizes the region where the total cross section increases with the energy, we shall consider here only the experimental data available above $\sqrt{s} = 20\,\mathrm{GeV}$ from pp and $\bar{p}p$ scattering. We note that this necessary threshold puts limitations in extensions of the formalism to other reactions, such as $\pi^{\pm}p$, $K^{\pm}p, \ldots$, due to the small number of experimental data available.

For the forward data on σ_{tot} and ρ, we use the Particle Data Group archives [3], to which we added the value of ρ and σ_{tot} at 1.8 TeV obtained by the E811 Collaboration [4]. The statistical and systematic errors were added in quadrature. We did not include the cosmic-ray information on the pp total cross sections due to the model dependences involved [6].

The differential cross section data include the optical point,

$$\left[\frac{\mathrm{d}\sigma(s,q^2)}{\mathrm{d}q^2}\right]_{q^2=0} = \frac{\sigma^2_{\mathrm{tot}}(1+\rho^2)}{16\pi}\,, \qquad (15)$$

and the data above the Coulomb–nuclear interference region, namely $q^2 > 0.01\,\mathrm{GeV}^2$. The data include 12 sets from pp scattering, at $\sqrt{s} = 23.5$, 27.4, 30.7, 44.7, 52.8, and 62.5 GeV and from $\bar{p}p$ scattering, at $\sqrt{s} = 31$, 53, 61, 546, 630 and 1800 GeV. The pp data at 27.4 GeV, covering the region $5.5 \le q^2 \le 14\,\mathrm{GeV}^2$, are from [21]. The $\bar{p}p$ differential cross section data at 1.8 TeV include those obtained by the E710 Collaboration [8] ($0.045 \le q^2 \le 0.627\,\mathrm{GeV}^2$) and by the CDF Collaboration [22] ($0.035 \le q^2 \le 0.285\,\mathrm{GeV}^2$). In this case we used two optical points with the values of σ_{tot} and ρ from [4] (E811 Collaboration) and [8] (E710 Collaboration). The complete list of references to the other data sets can be found in [1] ([26, 28–31]). In all these sets the experimental errors correspond to the statistical ones.

We note that we have used all the experimental data referred to before, that is, we did not perform any kind of data selection in the above standard ensemble.

3.2 Fitting and results

As recalled in Sect. 2.2, the applicability of the dispersion relations, outside the forward direction, depends on the maximum value of the momentum transfer considered. For this reason, we shall treat separately fits to only forward quantities, $\sigma_{\rm tot}$ and ρ, and simultaneous fits to these quantities plus the differential cross section data. We first present the fits to the forward data and next discuss the applicability of the dispersion techniques beyond the forward direction.

3.2.1 Fits to the forward scattering data

Making use of the formalism described in Sect. 2, we performed simultaneous fits to $\sigma_{\rm tot}$ and ρ data, above 20 GeV, from pp and $\bar{p}p$ scattering. Since we are treating here only forward data ($q^2 = 0$), the sole parameters involved are those associated with $\alpha_i(s)$ and $\bar{\alpha}_i(s)$ in (6) and (8).

The fits were performed through the CERN-Minuit code, with the estimated errors in the free parameters corresponding to an increase of the χ^2 by one unit. For this ensemble of data good statistical results were obtained with only one exponential factor ($n = 1$ in (5) and (7)) and the best fit indicated $\chi^2/{\rm DOF} = 1.07$ for 83 degrees of freedom. The constraint (9) in this case reduces to $C_1 = \bar{C}_1$ and the fit indicated a value of the subtraction constant compatible with zero. The numerical results are displayed in Table 1 and the corresponding curves, together with the experimental data analyzed, are shown in Fig. 6.

These results will be discussed in detail in Sect. 4, but we note here the good quality of the fit in terms of the $\chi^2/{\rm DOF}$ and also the small number of free parameters involved: 5. We also note a crossing in the total cross sections, with $\sigma_{\rm tot}^{pp}$ becoming higher than $\sigma_{\rm tot}^{\bar{p}p}$ above $\sqrt{s} \approx 100\,{\rm GeV}$, and a similar effect is predicted for $\rho(s)$. As we recalled in Sect. 2.1, these behaviors do not violate any high-energy theorem on elastic hadron scattering. However, the result for $\rho^{\bar{p}p}(s)$ is below the experimental data available at the highest energies. We shall discuss this effect in Sect. 4.2.

3.2.2 Fits beyond the forward direction

We now consider simultaneous fits to $\sigma_{\rm tot}(s)$, $\rho(s)$ and ${\rm d}\sigma(s,q^2)/{\rm d}q^2$, from pp and $\bar{p}p$ scattering. As recalled before, although dispersion relations have been used even in the region of medium and large momentum transfer (see, for example, [18, 23–26]), an important point concerns the exact region in the q^2 variable inside which dispersion relations hold. In what follows we first review some formal results involved which show us that, in the case of pp and $\bar{p}p$ scattering (and nucleon–nucleon in general), the situation is not simple or neat. Based on these results we shall infer a reasonable strategy, not proved to be wrong, that will allow us to develop simultaneous fit procedures including the differential cross section data. Note that, since we are treating with a sub-class of entire functions in the logarithm of the energy, the discussion that follows applies equally well to both integral and derivative dispersion relations [19].

Table 1. Results of the simultaneous fits to $\sigma_{\rm tot}$ and ρ from pp and $\bar{p}p$ scattering. All the parameters are in GeV^2, $\chi^2/{\rm DOF} = 1.07$ for 83 degrees of freedom and $C_1 = \bar{C}_1$

	pp scattering		$\bar{p}p$ scattering
A_1	121.9 ± 2.7	$\bar{A}_1$	140.8 ± 3.6
B_1	-9.82 ± 0.72	$\bar{B}_1$	-11.78 ± 0.86
C_1	1.036 ± 0.049	$\bar{C}_1$	1.036 ± 0.049

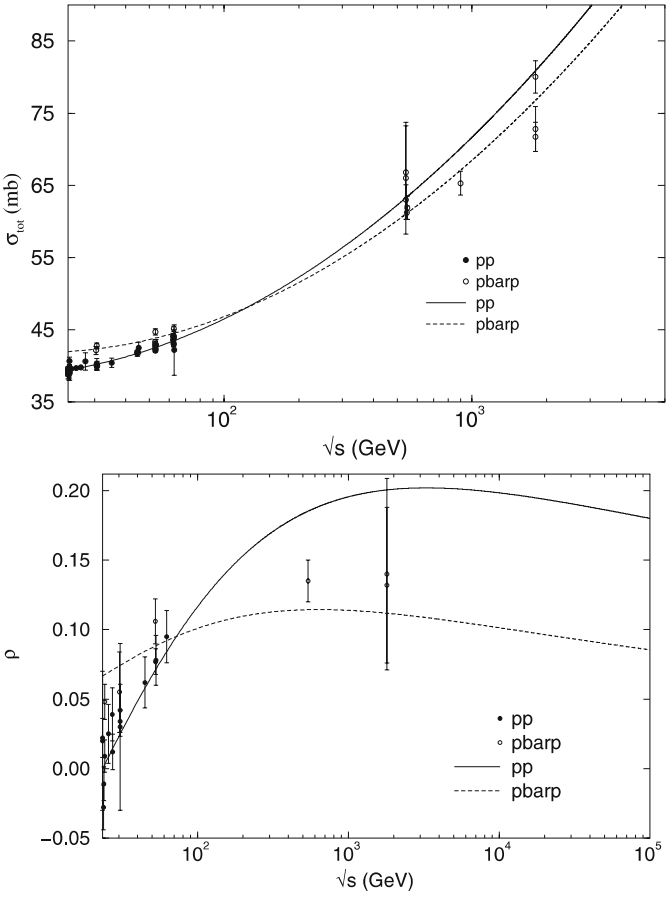

Fig. 6. Fit results to the forward data, $\sigma_{\rm tot}$ and ρ, from pp and $\bar{p}p$ scattering

Analyticity in q^2. Dispersion relations are connected with the unitarity and analyticity properties of the amplitude. Recently, the axiomatic approach to high-energy hadron scattering, as well as the rigorous analyticity–unitarity program have been nicely reviewed in the excellent papers by Vernov and Mnatsakanova [12] and Martin [13], where a complete list of references and credits to outstanding results and authors can be found. For this reason, based on these works, we shall only summarize and quote here the results, and as we understand it, give an updated view on the q^2-interval inside which dispersion relations hold. The results are the following.

1. For meson–meson and meson–nucleon scattering, a rigorous formalism based on local field theory allows one to prove that dispersion relations are valid in fi-

nite intervals of the momentum transfer. For example, $q^2_{\rm max} = 32m^2_\pi/3 \approx 0.2\,{\rm GeV}^2$ in the case of πN scattering [12] and $q^2_{\rm max} = 28m^2_\pi \approx 0.55\,{\rm GeV}^2$ in the case of $\pi\pi$ scattering [13].
2. Similar intervals can be deduced for other processes, like $\gamma + N \to \gamma + N^{(\star)}$, $\gamma + N \to \pi + N^{(\star)}$, $e + N \to e + \pi + N^{(\star)}$ [13].
3. In the formal analyticity–unitarity context there seems to be no results for nucleon–nucleon scattering. However, a limit $q^2_{\rm max} = m^2_\pi/4 \approx 0.005\,{\rm GeV}^2$ can be inferred from perturbation theory [13].
4. The reason why elastic pp and $\bar{p}p$ amplitudes "lack the usual analytical properties is that the cut in the complex s plane starts from $s_0 = 4m^2$ (due to the virtual annihilation process), while the physical region of $\bar{p}p$ scattering starts from $s_1 = 4M^{2}$" [12]. Here m corresponds to the pion mass and M to the proton mass.
5. In the context of the double-dispersion representation by Mandelstam [27], the domain in the q^2 variable, inside which dispersion relations hold for a process $m + m \to m + m$, extends up to $q^2_{\rm max} = 9m^2$ [28]. Although the original approach treated only pion–pion scattering, one point to stress is the fact that for all mass cases this representation was never proved nor disproved in the contexts of the axiomatic field theory or perturbation theory [13].

We also recall that fixed-q^2 dispersion relations for nucleon–nucleon scattering have been used by Kroll and co-authors [24, 25] and in particular, in [24], pp and $\bar{p}p$ scattering were investigated through dispersion relations in the region $0 \le q^2 \le 3\,{\rm GeV}^2$. However, there is no reference to a formal numerical value for $q^2_{\rm max}$.

These are the results we have found and compiled on the applicability of dispersion relations beyond the forward direction. We understand that the quoted bound from perturbation theory seems too unreliable to be considered in the case of a soft processes like elastic pp and $\bar{p}p$ scattering. A second aspect concerns the fact that, in the context of the axiomatic field theory, the Mandelstam representation for all mass cases was never proved to be incorrect (or correct either). If the representation can be extended to the pp and $\bar{p}p$ case, the analyticity domain could cover the region up to $q^2_{\rm max} = 9m^2_p \approx 8\,{\rm GeV}^2$.

Strategies and fits. Based on the above information, we understand that it can be instructive to perform tests on distinct values for $q^2_{\rm max}$ and investigate the consequences in the description of the bulk of the experimental data on $\sigma_{\rm tot}(s)$, $\rho(s)$ and ${\rm d}\sigma(s,q^2)/{\rm d}q^2$, from pp and $\bar{p}p$ scattering. Since the typical mass scale in the hadronic scattering is the proton mass (which is also expected to represent an interface between soft and semihard processes), it may be reasonable and perhaps even conservative to consider some bounds $q^2_{\rm max}$ inside the region 1–2 GeV^2. Moreover, it seems also important to address the practical applicability of the dispersion approach at medium and large values of the momentum transfer by taking into account all the differential cross section data available, namely, $q^2_{\rm max} = 14\,{\rm GeV}^2$. Despite the lack of a formal justification for this extreme case, we understand that it may also be useful to get some additional information on the regions where dispersion relations work, even if only in a strictly phenomenological context. It is important to stress that the strategy to consider different values for $q^2_{\rm max}$ is only an ansatz and that the main point in favor of this hypothesis is the fact that there is no formal proof against it, or in other words, we understand that it should not constitute a serious formal drawback. Based on the above discussion, we shall consider four variants for the fits by selecting differential cross section data up to $q^2_{\rm max} = 1.0$, 1.5, 2.0 and 14 GeV^2. As before, the fits were performed through the Minuit code. For this ensemble of data, independently of the value considered for $q^2_{\rm max}$, the best results demanded three exponential terms in the imaginary part of the amplitude and therefore 30 free parameters to be fitted. The constraint (9) was taken into account by defining $C_1 = \bar{C}_1 + \bar{C}_2 + \bar{C}_3 - C_2 - C_3$.

Table 2. Statistical information on the fit results to $\sigma_{\rm tot}$, ρ and ${\rm d}\sigma/{\rm d}q^2$ data from pp and $\bar{p}p$ scattering in different intervals of the momentum transfer variable

$q^2_{\rm max}$ in GeV^2	NDOF	χ^2/DOF
1.0	923	2.476
1.5	1003	2.909
2.0	1064	2.881
14.0 (all data)	1277	2.829

The χ^2 information on each of the four variants considered is displayed in Table 2. We note that the χ^2/DOF lies in the interval 2.5–3.0 for a number of degrees of freedom equal or greater than 923. It is important to mention that these values are typical of global fits to the experimental data on $\sigma_{\rm tot}(s)$, $\rho(s)$ and ${\rm d}\sigma(s,q^2)/{\rm d}q^2$, from pp and $\bar{p}p$ scattering [29]. The "large" values are the consequences of several points in the differential cross sections that lie outside a normal distribution, as well as different normalizations from different experiments in distinct kinematic intervals. As commented before, we did not perform any kind of data selection. In fact, despite the large values of the χ^2/DOF, the visual description of the experimental data is good in all the cases investigated. In particular we display here the results for $q^2_{\rm max} = 2\,{\rm GeV}^2$, which we understand can be considered a conservative case (in agreement with the expected analyticity interval in terms of the momentum transfer) and for $q^2_{\rm max} = 14\,{\rm GeV}^2$. The values of the free parameters in both cases are shown in Table 3 and the corresponding curves together with the experimental data analyzed in Figs. 7 and 8 ($q^2_{\rm max} = 2\,{\rm GeV}^2$) and Figs. 9 and 10 ($q^2_{\rm max} = 14\,{\rm GeV}^2$). We see that the description of all the differential cross section data is quite good, even in the extreme case $q^2_{\rm max} = 14\,{\rm GeV}^2$.

4 Discussion

In this section we first summarize the main results we have obtained and then proceed with a discussion of their physical implications and their applicabilities in the experimen-

Table 3. Results of the simultaneous fits to $\sigma_{\rm tot}$, ρ and $\mathrm{d}\sigma/\mathrm{d}q^2$ from pp and $\bar{p}p$ scattering, with differential cross section data up to $q^2_{\rm max} = 2.0\,\mathrm{GeV}^2$ and $q^2_{\rm max} = 14\,\mathrm{GeV}^2$, for which $K = 49.7 \pm 1.7$ and $K = -0.1053 \pm 0.0048$, respectively. All the parameters are in GeV^2 and $C_1 = \bar{C}_1 + \bar{C}_2 + \bar{C}_3 - C_2 - C_3$

	pp scattering			$\bar{p}p$ scattering	
	$q^2_{\rm max} = 2.0\,\mathrm{GeV}^2$	$q^2_{\rm max} = 14\,\mathrm{GeV}^2$		$q^2_{\rm max} = 2.0\,\mathrm{GeV}^2$	$q^2_{\rm max} = 14\,\mathrm{GeV}^2$
A_1	91.13 ± 0.28	109.70 ± 0.28	$\bar{A}_1$	119.61 ± 0.44	112.28 ± 0.44
B_1	-12.939 ± 0.039	-16.529 ± 0.039	$\bar{B}_1$	-2.486 ± 0.073	-0.468 ± 0.074
C_1	constrained	constrained	$\bar{C}_1$	-0.0174 ± 0.0038	-0.1673 ± 0.0039
D_1	-7.79 ± 0.33	-8.91 ± 0.32	$\bar{D}_1$	3.134 ± 0.067	3.170 ± 0.069
E_1	2.908 ± 0.051	3.045 ± 0.050	$\bar{E}_1$	0.4884 ± 0.0078	0.4860 ± 0.0082
A_2	16.82 ± 0.22	-4.06 ± 0.23	$\bar{A}_2$	14.51 ± 0.15	10.23 ± 0.15
B_2	7.071 ± 0.030	11.387 ± 0.030	$\bar{B}_2$	-6.730 ± 0.024	-6.756 ± 0.027
C_2	0.3027 ± 0.0047	0.0952 ± 0.0047	$\bar{C}_2$	0.9035 ± 0.0027	0.9613 ± 0.0029
D_2	1.647 ± 0.014	1.290 ± 0.014	$\bar{D}_2$	-1.549 ± 0.011	-1.476 ± 0.013
E_2	0.4646 ± 0.0022	0.5097 ± 0.0023	$\bar{E}_2$	0.5521 ± 0.0011	0.5645 ± 0.0012
A_3	0.2582 ± 0.0049	1.0554 ± 0.0077	$\bar{A}_3$	-17.160 ± 0.055	-8.148 ± 0.031
B_3	-0.09894 ± 0.00074	-0.3607 ± 0.0013	$\bar{B}_3$	2.6083 ± 0.0060	1.2313 ± 0.0040
C_3	$0.5921\mathrm{E}{-02} \pm 0.0070\mathrm{E}{-02}$	0.02372 ± 0.00012	$\bar{C}_3$	-0.11298 ± 0.00038	-0.05572 ± 0.00025
D_3	0.303 ± 0.019	0.6454 ± 0.0081	$\bar{D}_3$	1.5672 ± 0.0084	0.9272 ± 0.0072
E_3	0	0.0176 ± 0.0011	$\bar{E}_3$	0	0.03859 ± 0.0011

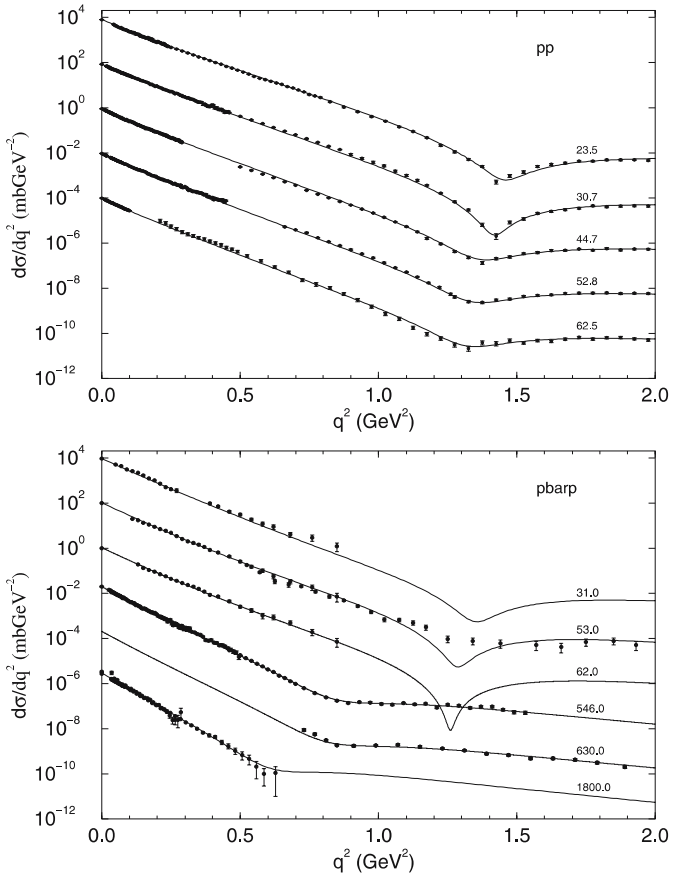

Fig. 7. Differential cross sections from global fits to pp and $\bar{p}p$ data with $q^2_{\rm max} = 2\,\mathrm{GeV}^2$. Curves and data were multiplied by factors of 10 ± 2

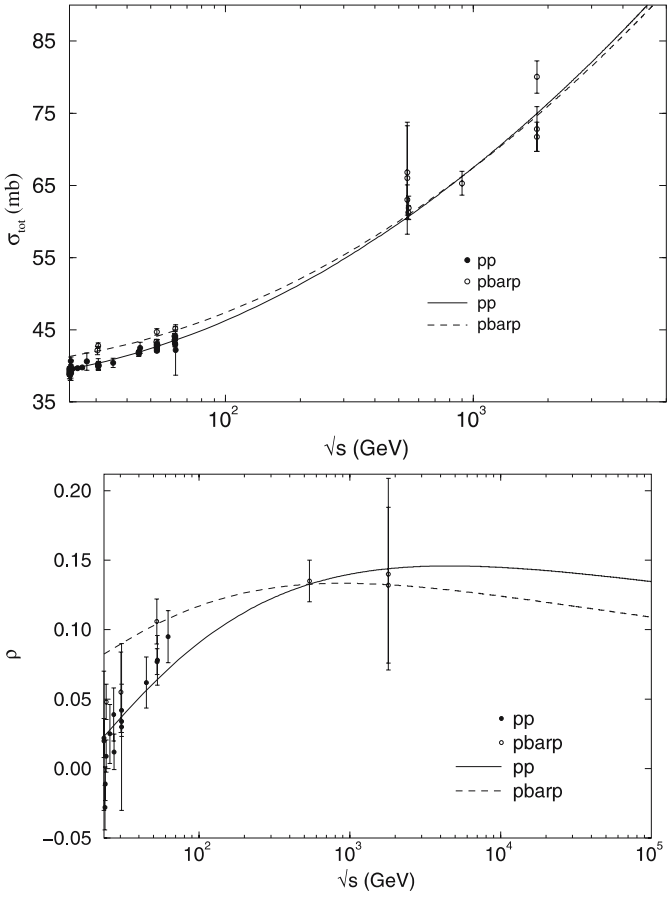

Fig. 8. Total cross section and ρ from global fits to pp and $\bar{p}p$ data with differential cross section data up to $q^2_{\rm max} = 2\,\mathrm{GeV}^2$

tal and phenomenological contexts. By means of a novel essentially model-independent analytical parameterization for the scattering amplitude and fits to physical quantities that characterize the elastic pp and $\bar{p}p$ scattering, we have developed a predictive formalism in the variables s and q^2 that has only empirical and formal bases. The ap-

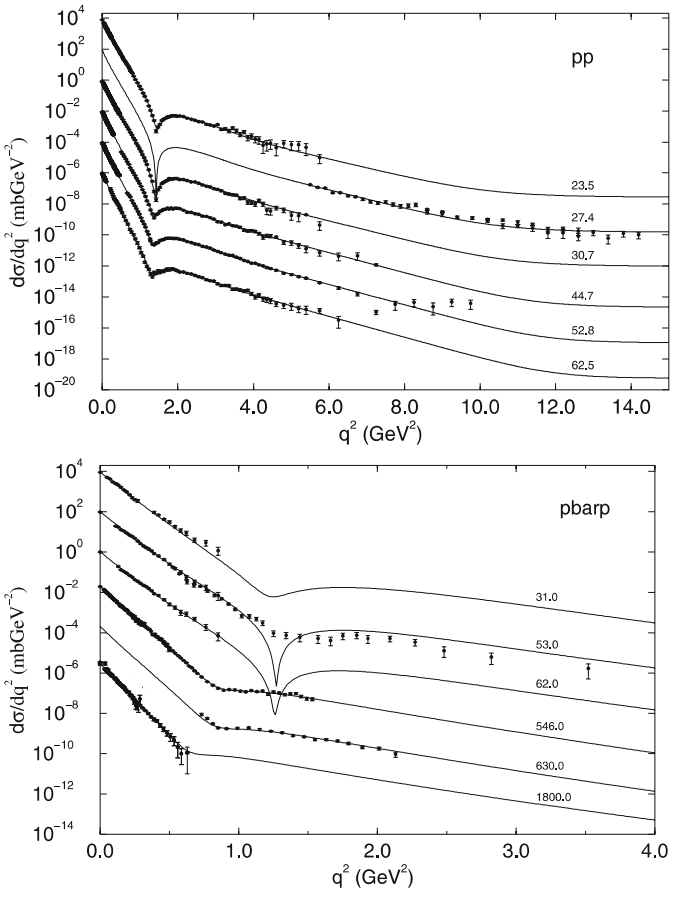

Fig. 9. Differential cross sections from global fits to pp and $\bar{p}p$ data with $q^2_{\max} = 14\,\mathrm{GeV}^2$ (all differential cross section data). Curves and data were multiplied by factors of 10 ± 2

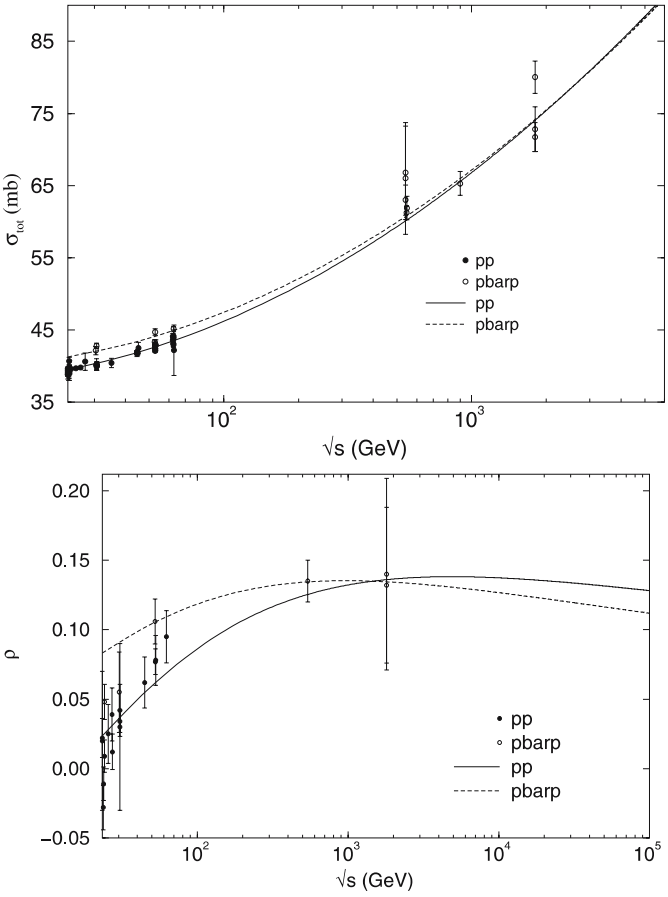

Fig. 10. Total cross section and ρ from global fits to pp and $\bar{p}p$ data with $q^2_{\max} = 14\,\mathrm{GeV}^2$ (all the differential cross section data)

proach is intended for the high-energy region, specifically above $\sqrt{s} = 20\,\mathrm{GeV}$ (in order to guarantee the empirical energy dependences). We first considered global fits to only the forward data, σ_{tot} and ρ, for which dispersion relations can be formally applied. We then included the differential cross section data and discussed strategies for the use of the dispersion relations, namely fits in different intervals in the momentum transfer variable: $q^2_{\max} = 1.0$, 1.5, 2.0 and $14\,\mathrm{GeV}^2$ (all data). The main point is the fact that there is no formal proof against these assumptions. Although we have displayed here only the results for $q^2 = 0$, $q^2_{\max} = 2$ and $q^2_{\max} = 14\,\mathrm{GeV}^2$, in all the cases investigated we have obtained good descriptions of the experimental data analyzed. As commented before, we consider the results with $q^2_{\max} = 14\,\mathrm{GeV}^2$ as an illustrative example on the practical applicability of the dispersion relations at medium and large values of the momentum transfer. However, a striking feature is the high quality of the data description reached in this case, as shown in Figs. 9 and 10.

In what follows, we discuss the applicability of the physical results in the experimental and phenomenological contexts. In the former case we shall consider processes that are being investigated or planned to be treated in accelerator experiments, referring to the following three cases: (1) pp scattering at $\sqrt{s} = 200\,\mathrm{GeV}$, that was investigated and might yet be investigated by the $pp2pp$ Collaboration at the Brookhaven RHIC; (2) $\bar{p}p$ scattering at $\sqrt{s} = 1.96\,\mathrm{TeV}$, that is being analyzed by the DZero Collaboration at the Fermilab Tevatron (RUN II); and (3) pp scattering at $\sqrt{s} = 14\,\mathrm{TeV}$, planned to be investigated by the TOTEM Collaboration at the CERN LHC. In the phenomenological context we shall make reference to some popular models which are, at the same time, representatives of different pictures to high-energy soft diffraction. To this end we will limit the discussion here only to the models by Desgrolard, Giffon and Predazzi (DGP) [29], Bourrely, Soffer and WU (BSW) [30], Donnachie and Landshoff (DL) [31], Block, Gregores, Halzen and Pancheri (BGHP) [32] and the odderon concept, introduced by Lukaszuk and Nicolescu [33].

We shall focus our discussion on the predictions obtained for $q^2 = 0$ (forward data only), $q^2_{\max} = 2\,\mathrm{GeV}^2$ and $q^2_{\max} = 14\,\mathrm{GeV}^2$. Also, we treat separately the results for the total cross section, the ρ parameter and the differential cross section, obtained from the above three variants of the fit procedure.

4.1 Total cross section

In the three fit variants, the results indicate a crossing with $\sigma^{pp}_{\mathrm{tot}}$ becoming greater than $\sigma^{\bar{p}p}_{\mathrm{tot}}$. However, the cross-

Table 4. Predictions for $\sigma_{\rm tot}(s)$ and $\rho(s)$ from fits to only forward data ($q^2 = 0$) and including the differential cross section data ($q^2_{\rm max} = 2\,{\rm GeV}^2$ and $q^2_{\rm max} = 14\,{\rm GeV}^2$)

Process	$q^2 = 0$		$q^2_{\rm max} = 2\,{\rm GeV}^2$		$q^2_{\rm max} = 14\,{\rm GeV}^2$	
	$\sigma_{\rm tot}$ (mb)	ρ	$\sigma_{\rm tot}$ (mb)	ρ	$\sigma_{\rm tot}$ (mb)	ρ
pp, $\sqrt{s} = 200$ GeV	52.27	0.1532	51.32	0.1439	51.12	0.1065
$\bar{p}p$, $\sqrt{s} = 1.96$ TeV	78.05	0.1114	75.74	0.1124	75.24	0.1343
pp, $\sqrt{s} = 14$ TeV	121.6	0.1964	107.5	0.1321	105.4	0.1365

ing point depends on the q^2-interval of the differential cross section data considered in the fit: $\sqrt{s} \approx 100\,{\rm GeV}$ for $q^2 = 0$, $\approx 500\,{\rm GeV}$ for $q^2_{\rm max} = 2\,{\rm GeV}^2$ and $\approx 3\,{\rm TeV}$ for $q^2_{\rm max} = 14\,{\rm GeV}^2$ as shown in Figs. 6, 8 and 10, respectively. That is, asymptotically, the difference $\Delta\sigma = \sigma^{\bar{p}p}_{\rm tot} - \sigma^{pp}_{\rm tot}$ does not goes to zero and as recalled in Sect. 2.1, this behavior is not in disagreement with formal results obtained in the context of axiomatic field theory.

Among the models quoted, this result suggest a dominant contribution of the odderon [33] at the highest energies. We stress that the only information we have introduced in our parameterization was the empirical fact that the pp and $\bar{p}p$ total cross sections increase at most as $\ln 2s$ (parameterizations for $\alpha_i(s)$ and $\bar{\alpha}_i(s)$ in (6) and (8)) and that the difference may increase at most as $\ln s$ (constraint (9)).

In particular, at $\sqrt{s} = 1.80\,{\rm TeV}$, the experimental results for $\sigma^{\bar{p}p}_{\rm tot}$ are characterized by the well known discrepancies between the values reported by the E811 and E710 Collaborations [4, 8] and that reported by the CDF Collaboration [34]. In this respect, except for the forward fit result for $\sigma^{\bar{p}p}_{\rm tot}$, which lies between the discrepant points Fig. 6, the predictions including the differential cross section data favor the E811/E710 results (Figs. 8 and 10).

In Table 4 we present our numerical predictions for the total cross sections in the case of the experiments referred to before. For pp scattering at 14 TeV (LHC) our results with $q^2_{\rm max} = 2\,{\rm GeV}^2$ and $q^2_{\rm max} = 14\,{\rm GeV}^2$ are in agreement, respectively, with the predictions from the BGHP model ($\sigma_{\rm tot} = 108.0 \pm 3.4\,{\rm mb}$) [32] and from the BSW model ($\sigma_{\rm tot} = 103.5\,{\rm mb}$) [30]. However, it should be noted that these models do not distinguish pp and $\bar{p}p$ scattering at asymptotic energies. The table also contains the results for $\rho(s)$, to be discussed in what follows.

4.2 The ρ parameter

As a consequence of the connections between real and imaginary parts of the amplitudes via dispersion relations, similar effects appear in our results for $\rho(s)$, as shown in Figs. 6, 8 and 10: $\rho^{pp}(s)$ becomes greater than $\rho^{\bar{p}p}(s)$ above $\sqrt{s} \approx 80\,{\rm GeV}(q^2 = 0)$, $\approx 200\,{\rm GeV}(q^2_{\rm max} = 2\,{\rm GeV}^2)$ and $\approx 2\,{\rm TeV}(q^2_{\rm max} = 14\,{\rm GeV}^2)$. In all the cases the constraint (9) assures the asymptotic behavior as $1/\ln s$ for both pp and $\bar{p}p$ scattering.

As in the case of the total cross section, these results are in agreement with the odderon dominance at the highest energies. A crossing in $\rho(s)$ with $\rho^{pp}(s)$ becoming greater than $\rho^{\bar{p}p}(s)$ is also predicted in one of the versions of the DGP model [29] and in the analysis of [6], which includes cosmic-ray information on $\sigma^{pp}_{\rm tot}$ and a model-dependent parameterization with odderon contribution.

Differently from the results for the total cross sections, we note here some distinct characteristics between the predictions for $\rho(s)$ obtained with only the forward data (Fig. 6) and those including the differential cross section data up to $q^2_{\rm max} = 2\,{\rm GeV}^2$ (Fig. 8) and $q^2_{\rm max} = 14\,{\rm GeV}^2$ (Fig. 10). In the former case the curve for $\rho^{\bar{p}p}(s)$ lies below the highest $\bar{p}p$ data, which does not occur when the differential cross section data are included. We have realized that this effect (Fig. 6 and partially in Fig. 8) is due to the large error bars of the experimental data at 1.8 TeV and also to the small number of ρ data from $\bar{p}p$ scattering above 20 GeV. In fact, at $\sqrt{s} = 1.8\,{\rm TeV}$, the experimental values are $\rho_{\rm E811} = 0.132 \pm 0.056$ [4] and $\rho_{\rm E710} = 0.140 \pm 0.069$ [8], corresponding to relative errors of 42% and 49%, respectively. For example, if we use the same central values and reduce the errors to 10%, the same fit leads to a curve that passes through the central values. However this is only technical information that certainly has nothing to do with a physical result in the context of our analysis. Experimentally it is known that, as the energy increases, it is very difficult to reach the Coulomb–nuclear interference region, from which the ρ parameter is extracted [2]. Therefore there is not expected an improvement in these experimental values, unless some novel technique could be developed. In this respect, the above effect, at the highest energies, cannot be eliminated in the present formulation and fit procedure, constituting, therefore, a drawback in our analysis, when only forward data are considered. However, comparison of Figs. 6, 8 and 10 shows an interesting effect: the quality of the visual description of the ρ data at the highest energies is improved with the addition of the differential cross section information.

The numerical predictions for $\rho(s)$, in the case of the experiments referred to before, and from the three fit variants ($q^2 = 0, q^2_{\rm max} = 2\,{\rm GeV}^2$ and $q^2_{\rm max} = 14\,{\rm GeV}^2$) are displayed in Table 4.

4.3 Differential cross section

As we have shown, the descriptions of the pp and $\bar{p}p$ differential cross section data analyzed are quite good for $q^2_{\rm max} = 2\,{\rm GeV}^2$ (Fig. 7) and even in the case of $q^2_{\rm max} = 14\,{\rm GeV}^2$ (Fig. 9). In this subsection we discuss the applicability of these results in the experimental and phenomenological contexts.

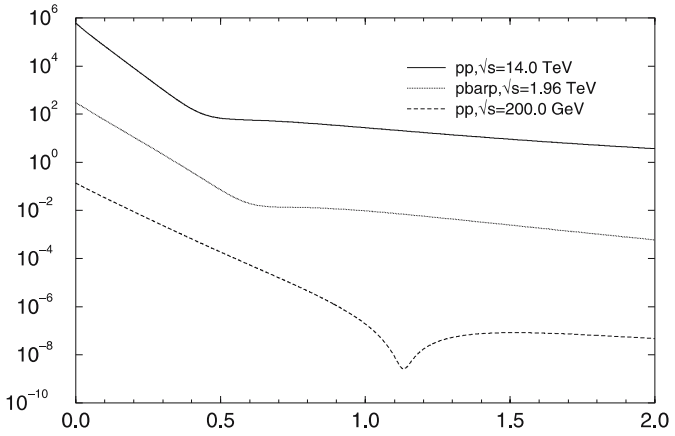

Fig. 11. Predictions for the differential cross sections at the RHIC, Tevatron and LHC energies from fits including the differential cross section data up to $q^2_{\rm max} = 2\,{\rm GeV}^2$ (Table 5). The upper and lower curves were multiplied by 10^3 and 10^{-3}, respectively

To the extent that our analysis can be considered model-independent and predictive, it may be instructive to detail the results for the experiments referred to in the beginning of this section. Our predictions for these processes, from the global fit including the differential cross section data up to $q^2_{\rm max} = 2\,{\rm GeV}$, are shown in Fig. 11, and the corresponding numerical results, in the region 0–2 $\rm GeV^2$, are displayed in Table 5 for some values of the momentum transfer. From Fig. 11 we note the presence of a dip at $q^2 \approx 1.2\,{\rm GeV}^2$ for pp scattering at 200 GeV and that the diffraction pattern becomes a shoulder at higher energies for both $\bar{p}p$ ($\sqrt{s} = 1.96\,{\rm TeV}$) and pp scattering ($\sqrt{s} = 14\,{\rm TeV}$); we also note the shrinkage of the diffraction peak as the energy increases.

4.3.1 Experimental aspects

As examples of practical use of these predictions in the experimental context, let us discuss the recent determinations of the slope parameter from elastic rates measured by the $pp2pp$ Collaboration (pp scattering at $\sqrt{s} = 200\,{\rm GeV}$) at the RHIC [35] and the preliminary results obtained by the DZero Collaboration ($\bar{p}p$ scattering at $\sqrt{s} = 1.96\,{\rm TeV}$) at the Tevatron [36]. Operationally, the differential cross section is expressed by

$$\frac{{\rm d}\sigma}{{\rm d}q^2} = \frac{1}{\mathcal{L}}\frac{{\rm d}N}{{\rm d}\,q^2},$$

where ${\rm d}N/{\rm d}q^2$ is the rate of the elastic interactions and $\mathcal{L}$ the machine luminosity. Due to uncertainties in the determination of $\mathcal{L}$ the above quoted experiments have extracted only the slope of the elastic rates, that is, the corresponding differential cross section could not yet be determined. In what follows we present our results for the corresponding slopes and discuss ways to contribute with a possible reasonable normalization of the elastic rates.

pp *at* $\sqrt{s} = 200\,{\rm GeV}$. In the case of the $pp2pp$ experiment, the slope B was obtained from the elastic rates measured in the q^2 range $0.010 \le q^2 \le 0.019\,{\rm GeV}^2$. The corresponding amplitude has contributions from the Coulomb amplitude, nuclear amplitude and the interference between them, and it is parameterized by [35]

$$\frac{{\rm d}\sigma}{{\rm d}t} = 4\pi(\hbar c)^2\left(\frac{\alpha G_E^2}{t}\right)^2 + \frac{1+\rho^2}{16\pi(\hbar c)^2}\sigma_{\rm tot}^2 {\rm e}^{-B|t|} - (\rho + \Delta\Phi)\frac{\alpha G_E^2}{|t|}\sigma_{\rm tot}{\rm e}^{-\frac{1}{2}B|t|}\ .$$

The fit parameters are the slope B and a normalization constant (elastic rates). The input values for $\sigma_{\rm tot}$ and ρ used by the authors were 51.6 mb (obtained from the Donnachie–Landshoff model) and 0.13 (fit by the UA4/2 Collaboration), respectively. The resulting slope parameter was

$$B = 16.3 \pm 1.6\ ({\rm stat.})\ \pm 0.9\ ({\rm syst.})\ {\rm GeV}^{-2}.$$

Adding in quadrature the error reads $\pm 1.8\,{\rm GeV}^{-2}$. From Fig. 4 we can see that this experimental value of the slope is above the general trend of the other measurements, even from $\bar{p}p$ scattering. This effect is due to the small values of the momentum transfer in which the measurement has been performed, namely lower than those in the other experiments and also because the interval is in the limit of the Coulomb–nuclear interference region ($q^2 \approx 0.01\,{\rm GeV}^2$). Since the pp data we have analyzed cover the region only up to $\sqrt{s} = 62.5\,{\rm GeV}$ and above $q^2 = 0.01\,{\rm GeV}^2$ (except for the optical point), it is an important test to check our predictions for the above quantity.

To this end, from the fit with $q^2_{\rm max} = 2\,{\rm GeV}^2$ and based on the experimental procedure [35], we have generated 19 differential cross section points, with estimated error of 1%, in the region $0.010 \le q^2 \le 0.019\,{\rm GeV}^2$ and fitted the points with an exponential form in the momentum transfer:

$$\frac{{\rm d}\sigma}{{\rm d}q^2} = A{\rm e}^{-Bq^2}, \qquad (16)$$

as shown in Fig. 12. With this procedure we have obtained

$$A = 136.0 \pm 1.7\,{\rm mbGeV}^{-2}\ ,$$
$$B = 14.46 \pm 0.84\,{\rm GeV}^{-2}\ ,$$

with $\chi^2/{\rm DOF} = 4.8 \times 10^{-5}$ for 17 degrees of freedom. Therefore, our result for the slope is in agreement with the experimental value, lying inside the lower error bar in the case that statistical and systematic errors are added in quadrature. The relative error with respect to the central value is 11%. Moreover, the input value used by the $pp2pp$ Collaboration, $\sigma_{\rm tot}^{pp} = 51.6\,{\rm mb}$, is also in agreement with our predictions for the cross section, as shown in Table 4, namely 51.32 mb. We also note that, although our results indicate $\rho = 0.1439$, which is higher than the input $\rho = 0.13$, this difference has no practical effect on the nuclear contribution in (16), since this parameter appears in

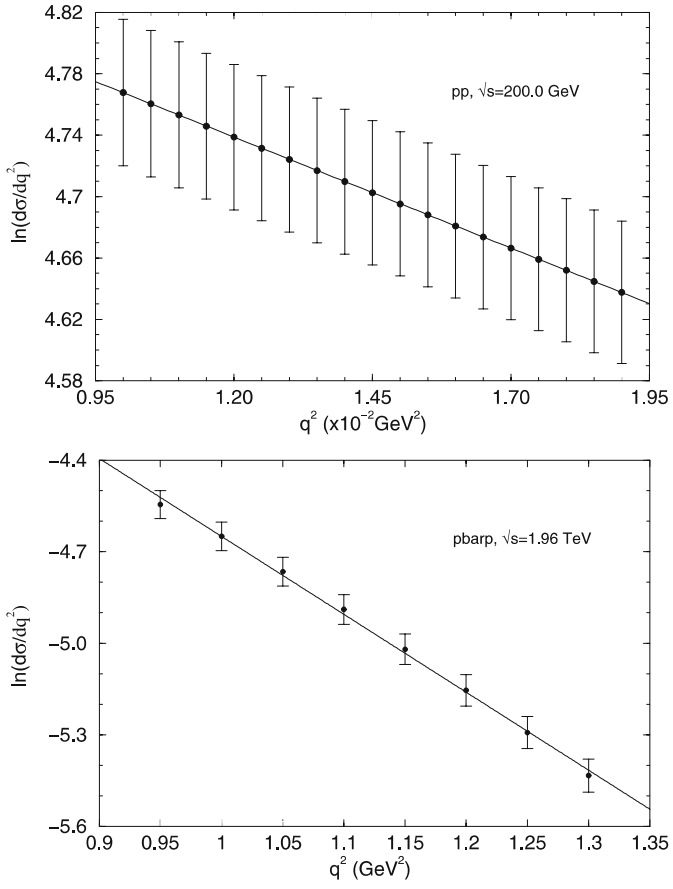

Fig. 12. Determination of the slope by means of an exponential fit, (16), to the generated differential cross section points, for $q^2_{\max} = 2\,\mathrm{GeV}^2$

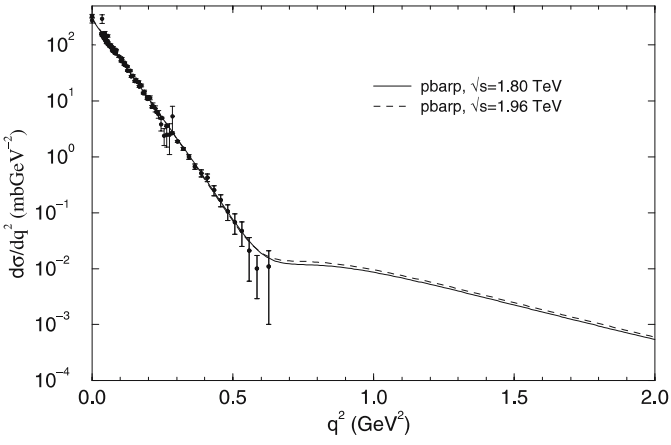

Fig. 13. Prediction for the $\bar{p}p$ differential cross section at $\sqrt{s} = 1.96\,\mathrm{TeV}$ and $\sqrt{s} = 1.80\,\mathrm{TeV}$, for $q^2_{\max} = 2\,\mathrm{GeV}^2$, together with the experimental data at $\sqrt{s} = 1.80\,\mathrm{TeV}$

the form $1 + \rho^2$. However that is not the case for the total cross section which has a quadratic contribution: σ^2_{tot}. We understand that these results corroborate the accuracy of our predictions and in this sense, the above value we obtained for the parameter A could be used as a suitable normalization factor in the estimation of the corresponding differential cross section.

$\bar{p}p$ at $\sqrt{s} = 1.96\,\mathrm{TeV}$. Now let us discuss the recent measurements (even if preliminary) of the elastic rates performed by the DZero Collaboration, from $\bar{p}p$ scattering at $\sqrt{s} = 1.96\,\mathrm{TeV}$ [36]. In this case, the rate of elastic collisions has been measured at medium values of the momentum transfer, in the interval $0.96 < q^2 < 1.31\,\mathrm{GeV}^2$ [37]. As an illustration, and for further discussion, our predictions for the differential cross section at $\sqrt{s} = 1.96\,\mathrm{TeV}$ and $\sqrt{s} = 1.80\,\mathrm{TeV}$, with $q^2_{\max} = 2\,\mathrm{GeV}^2$ are shown in Fig. 13 together with the experimental data, obtained by the E710 and CDF Collaborations, at $\sqrt{s} = 1.80\,\mathrm{GeV}$. In principle, the elastic rates at 1.96 TeV could be compared with the differential cross section data at 1.80 TeV, allowing for a kind of normalization. However, from Fig. 13, we see that the E710 data cover the region only up to $q^2 = 0.627\,\mathrm{GeV}^2$ and the main problem is the fact that in the gap between this last point and the first DZero point ($q^2 \approx 0.96\,\mathrm{GeV}^2$) the presence of a dip or a shoulder is expected, implying, in any case, a change of curvature. What is worst, the E710 point at $q^2 = 0.627\,\mathrm{GeV}^2$ has a large error bar (not shown in the figure, but taken into account in all the fits), making very difficult, in our opinion, any attempt to perform a reasonable normalization. In this respect, looking for more quantitative information and, as before, from the fit with $q^2_{\max} = 2\,\mathrm{GeV}^2$ and based on the experimental procedure [37], we have generated 8 differential cross section points with errors of 1%, in the region $0.95 \le q^2 \le 1.3\,\mathrm{GeV}^2$ and fitted the points with the exponential form, as shown in Fig. 12. In this case we have obtained

$$A = 0.123 \pm 0.004\,\mathrm{mb\,GeV}^{-2}\,,$$
$$B = 3.554 \pm 0.030\,\mathrm{GeV}^{-2}\,,$$

with $\chi^2/\mathrm{DOF} = 2.52$ for 6 degrees of freedom. We note that a close looking at the generated points in Fig. 12 shows that the last four points have a slope slightly greater than the first four points and this effect seems also to be present in the measured elastic rates [36, 37]. Although the experimental data are still being analyzed by the DZero Collaboration, we understand that the above information and the numerical results displayed in Table 5 can contribute with the discussion on a suitable normalization for these elastic rates. We shall return to this point in what follows.

4.3.2 Phenomenological aspects

We now turn the discussion to the phenomenological context, with main focus on the result we have obtained for the highest energy with differential cross section data available, namely $\bar{p}p$ scattering at $\sqrt{s} = 1.80\,\mathrm{TeV}$; see Fig. 13. The point is to compare this result with predictions from the models referred to in the beginning of this section.

From Fig. 13, our result indicates a change of curvature in the region of the last three experimental points ($q^2 \approx 0.55$–$0.65\,\mathrm{GeV}^2$) with a shoulder shape and not a dip

Table 5. Predictions for the differential cross sections in mbGeV^{-2} at the RHIC, Tevatron and LHC energies, from global fits including the differential cross section data up to $q^2_{\rm max} = 2.0\,{\rm GeV}^2$

q^2 in GeV^2	pp, $\sqrt{s} = 200$ GeV	$\bar{p}p$, $\sqrt{s} = 1.96$ TeV	pp, $\sqrt{s} = 14$ TeV
0.00	136.24	298.18	602.87
0.01	117.66	251.98	470.45
0.05	66.649	129.03	190.54
0.10	33.576	56.399	65.903
0.15	17.144	24.839	23.222
0.20	8.8167	10.982	8.2384
0.25	4.5585	4.8519	2.9339
0.30	2.3699	2.1307	1.0537
0.35	1.2400	0.92503	0.39265
0.40	0.65358	0.39539	0.16557
0.45	0.34731	0.16687	0.090879
0.50	0.18607	0.071284	0.067705
0.55	0.10042	0.033293	0.060450
0.60	0.054478	0.019393	0.057098
0.65	0.029605	0.014952	0.054020
0.70	0.016034	0.013790	0.050435
0.75	0.0085958	0.013451	0.046423
0.80	0.0045185	0.013078	0.042242
0.85	0.0022989	0.012456	0.038117
0.90	0.0011103	0.011606	0.034201
0.95	0.00049312	0.010614	0.030578
1.00	0.00018982	0.0095647	0.027284
1.05	5.5411E-05	0.0085216	0.024324
1.10	8.5222E-06	0.0075277	0.021686
1.15	3.9878E-06	0.0066078	0.019345
1.20	1.7294E-05	0.0057734	0.017276
1.25	3.5677E-05	0.0050275	0.015449
1.30	5.2974E-05	0.0043677	0.013838
1.35	6.6641E-05	0.0037883	0.012417
1.40	7.6041E-05	0.0032825	0.011164
1.45	8.1462E-05	0.0028425	0.010058
1.50	8.3576E-05	0.0024608	0.0090810
1.55	8.3151E-05	0.0021304	0.0082164
1.60	8.0907E-05	0.0018448	0.0074507
1.65	7.7458E-05	0.0015981	0.0067714
1.70	7.3291E-05	0.0013851	0.0061679
1.75	6.8779E-05	0.0012013	0.0056310
1.80	6.4189E-05	0.0010426	0.0051523
1.85	5.9707E-05	0.00090562	0.0047250
1.90	5.5453E-05	0.00078734	0.0043428
1.95	5.1497E-05	0.00068517	0.0040002
2.00	4.7875E-05	0.00059687	0.0036928

(minimum) with defined position. This effect is due to the contribution from the real part of the amplitude as shown in Fig. 14, where we display separately the contributions to the differential cross section from only the real and only the imaginary parts of the amplitudes in the cases of $q^2_{\rm max} = 2\,{\rm GeV}^2$ and $q^2_{\rm max} = 14\,{\rm GeV}^2$. From this figure we see that, as expected, the imaginary part presents a zero (change of sign) and inside this region, the value of the minimum in the differential cross section is due to the contribution of the real part (a shoulder in this case). The real part of the amplitude also presents a zero at $q_0^2 \approx 0.30\,{\rm GeV}^2$ in the case of $q^2_{\rm max} = 2\,{\rm GeV}^2$ and $q_0^2 \approx 0.38\,{\rm GeV}^2$ for $q^2_{\rm max} = 14\,{\rm GeV}^2$. These results for the real part are in agreement with a theorem demonstrated by Martin, which states that the real part changes sign at $q^2 > 0.1\,{\rm GeV}^2$ [38].

On the other hand, the contributions from the imaginary parts are very similar in both cases, indicating a zero at $q_0^2 \approx 0.70\,{\rm GeV}^2$ for $q^2_{\rm max} = 2\,{\rm GeV}^2$ and at $q_0^2 \approx 0.73\,{\rm GeV}^2$ for $q^2_{\rm max} = 14\,{\rm GeV}^2$. Therefore, from this figure, we can infer with some certainty that the position of the first minimum in the differential cross section at this energy occurs at $q_0^2 = 0.70\,{\rm GeV}^2$ ($q^2_{\rm max} = 2\,{\rm GeV}^2$). In the phenomenological context this value is in agreement with the predictions of the DGP, BSW and DL models, but not with that from

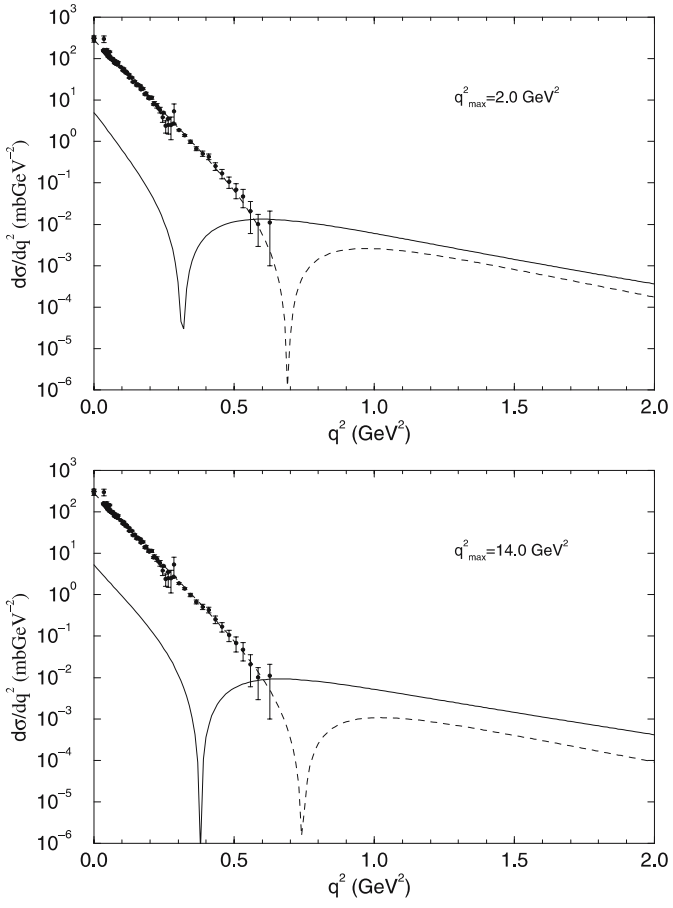

Fig. 14. Contributions to the $\bar{p}p$ differential cross section at $\sqrt{s} = 1.80\,\text{TeV}$ from the real (*solid*) and imaginary (*dashed*) parts of the amplitude for $q^2_{\max} = 2\,\text{GeV}^2$ and $q^2_{\max} 14\,\text{GeV}^2$

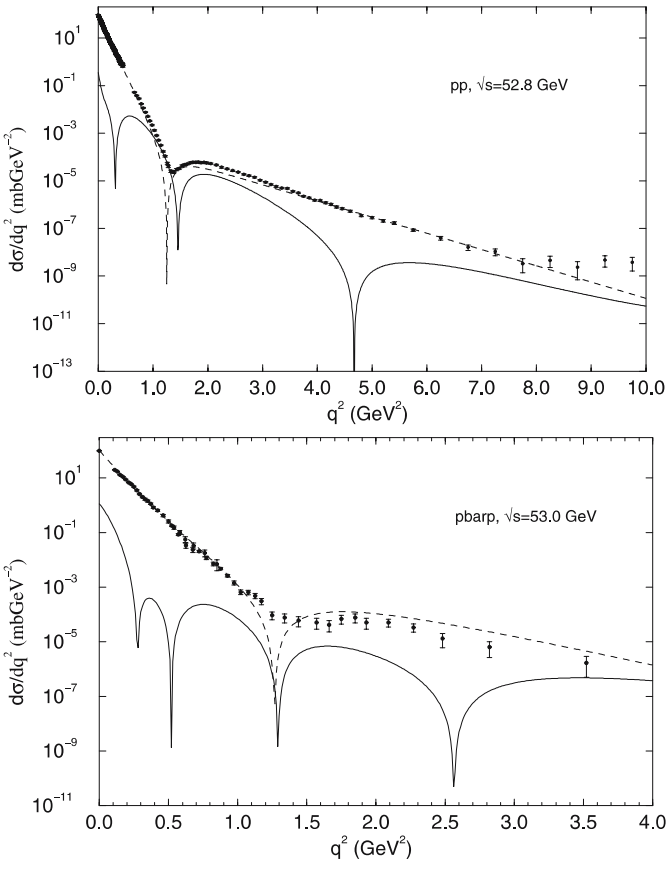

Fig. 15. Contributions to the differential cross section from the real (*solid*) and imaginary (*dashed*) parts of the amplitude for $q^2_{\max} = 14\,\text{GeV}^2$

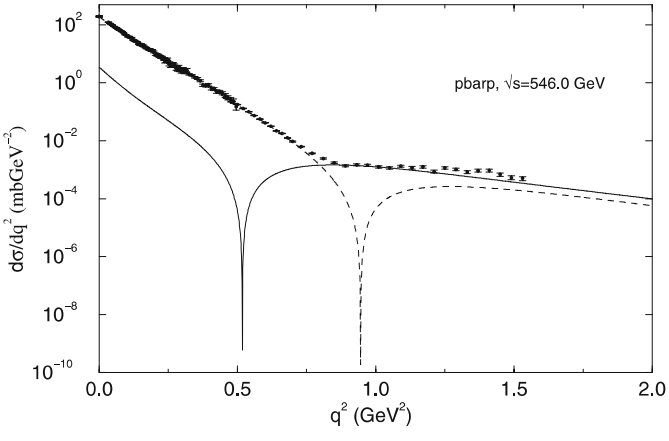

Fig. 16. Contributions to the differential cross section from the real (*solid*) and imaginary (*dashed*) parts of the amplitude for $q^2_{\max} = 14\,\text{GeV}^2$

the BGHP model, since the minimum in this model is predicted to be at $q_0^2 \approx 0.60\,\text{GeV}^2$ (coincident with the highest E710 point). We think that this is an important point that should be carefully analyzed, when comparing elastic rates with model predictions at $\sqrt{s} = 1.96\,\text{TeV}$.

Another aspect to note in Fig. 14 is that, in both cases, the contribution of the imaginary part dominates in the region of small momentum transfer, up to the beginning of the shoulder. On the other hand, in this region and for higher values of the momentum transfer, it is the contribution of the real part that dominates. However, in order to investigate this effect in more detail, we must consider the region of medium and large momentum transfer, that is, the results of the fits with $q^2_{\max} = 14\,\text{GeV}^2$. We stress that, even under restrictive formal justification, our results taking into account all the differential cross section data are quite good, as shown in Fig. 9, and therefore it may be instructive to discuss the implications of this variant of the fit.

Concerning the contributions to the differential cross sections from the real and the imaginary parts of the amplitude, we consider three typical examples: the results for pp scattering at 52.8 GeV and $\bar{p}p$ at 53 GeV, shown in Fig. 15, and those for $\bar{p}p$ at 546 GeV, displayed in Fig. 16, together with the corresponding experimental data. The point is that, according to our predictions, in the energy region of the CERN ISR ($\sqrt{s} \approx 23$–$63\,\text{GeV}$), the imaginary part dominates at medium and large values of the momentum transfer (Fig. 15). On the other hand, at higher energies, such as the regions of the CERN Collider (Fig. 16) and Tevatron (Fig. 14), it is the contribution from the real part that dominates.

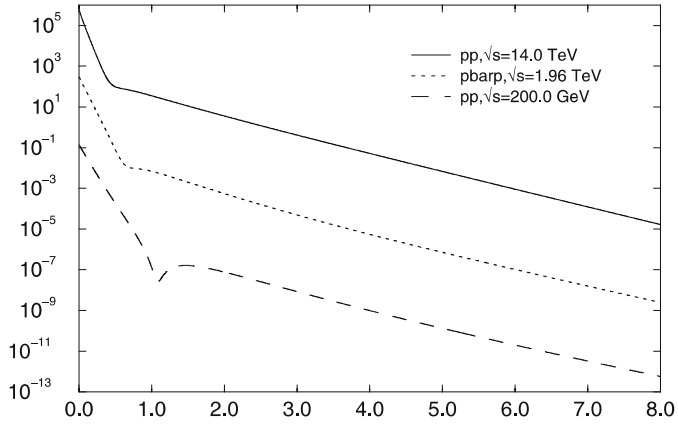

Fig. 17. Predictions for the differential cross sections at the RHIC, Tevatron and LHC energies from fits including the differential cross section data up to $q^2_{\rm max} = 14\,{\rm GeV}^2$ (all data). The upper and lower curves were multiplied by 10^3 and 10^{-3}, respectively

Finally, it may also be instructive to see what kind of results can be predicted in the region of large momentum transfer at the RHIC, Tevatron and LHC energies. We display these in Fig. 17 up to $q^2 = 8\,{\rm GeV}^2$, the interval generally considered in the publications. The main point here is the prediction of a smooth decrease of the differential cross section above the first minimum, without secondary structures in this region. Among the quoted phenomenological approaches, this behavior is predicted only in the DL model. However, we note from Fig. 9 that a small change in the curvature is predicted at $q^2 \approx 12\,{\rm GeV}^2$.

5 Conclusions and final remarks

We have introduced an analytical parameterization for the elastic hadron–hadron scattering amplitude and a fit procedure characterized by at least five important novel aspects: (1) the parameterization is almost model-independent, with enclosed dependences on the energy and momentum extracted from the empirical behavior of the experimental data and in agreement with some high-energy theorems and bounds from AQFT; (2) the real and imaginary parts of the amplitude are entire functions of the logarithm of the energy s and are connected through derivative dispersion relations; (3) the pp and $\bar{p}p$ scattering are also connected to the extent that analyticity and unitarity lead to dispersion relations; (4) the approach is predictive in both energy and momentum variables; (5) fits to pp and $\bar{p}p$ experimental data, above 20 GeV, on the forward quantities and then including differential cross sections, allow for good global descriptions of all the data, even in different regions of the momentum transfer.

We have presented a critical remark on a drawback that still remains in the present formulation, which is related to the results for $\rho^{\bar{p}p}(s)$, in the particular case of a forward fit. One way to address this question may be to consider the derivative dispersion relations up to second or third order in the tangent operator. Results in this direction will be reported elsewhere.

Another aspect that deserves some comment is the number of free parameters involved in the analysis. When including the differential cross section data, even in the region $q^2 \leq 1\,{\rm GeV}^2$, the fit demands 3 exponentials in the imaginary part of the amplitude and therefore 30 free fit parameters. We understand that this cannot be seen as an disadvantage of the formalism in terms of a large number of parameters. In fact, we are not treating a theoretical model but, on the contrary, a model-independent approach aimed to describe and predict the physical quantities of interest on empirical and formal grounds. Therefore, the number of parameters does not matter and, in this context, it can be as large as it is needed.

In this analysis we made use of the standard sets of experimental data on pp and $\bar{p}p$ scattering above 20 GeV (referred to in Sect. 3.1), without any kind of data selection. As commented, this strategy explains the large values of the χ^2/DOF in the fits. However, it is important to mention that recent analyses point out the necessity of some screening criterion in order to avoid spurious data, normalization problems and other effects in both forward and non-forward data [39, 40]. All that could improve the quality of the fits and will be subject of future investigation.

We also note that we did not use any model information in the construction of the parameterizations (5)–(8): they were inferred only with basis on the empirical behavior of the experimental data above 20 GeV. However, from a phenomenological point of view, it is expected that some contributions from lower energies may still be present at the above threshold (for example, secondary mesonic exchanges in a Regge context [41]). Therefore it may be interesting to test additional terms in our original parameterization, that could simulate these effects, from an empirical point of view, and investigate the consequences in the description of the experimental data.

We now summarize some results that we understand are topical in this analysis. The behavior of the forward quantities, $\sigma_{\rm tot}(s)$ and $\rho(s)$, from pp and $\bar{p}p$ scattering are characterized by crossing effects, which are typical of odderon contributions. A relevant result is the prediction that ρ^{pp} becomes higher than $\rho^{\bar{p}p}$ above $\sqrt{s} \approx 80\,{\rm GeV}$, a result that might be verified in the short term at the RHIC by the $pp2pp$ Collaboration. Our results for the differential cross section at the Tevatron energies are in agreement with the predictions from the majority of the models, except that by Block et al. [32], in what concerns the position of the first minimum. We have also discussed the applicability of our numerical results in the normalization of elastic rates. We add that, if we consider the fit including all the differential cross section data, the DL model is favored, since no structures are predicted in the region of large momentum transfer.

In closing we should stress that, despite the encouraging results we have reached, this phenomenological analysis constitutes a first attempt in the search of a formally rigorous and predictive model-independent approach. Much more research must still be done along several lines, as for example, a complete check on all the high-energy

theorems and bounds, to establish the exact interval in the momentum transfer variable in which dispersion relations hold (or another framework for evaluation of the real part of the amplitude), studies on the effect of higher orders in the derivative dispersion relations and a systematic investigation on the influence of data selection. We hope that the results here presented can contribute with further developments along these aspects.

Acknowledgements. For financial support R.F.A. and M.J.M. are thankful to FAPESP (Contracts No. 03/00228-0 and No. 04/10619-9) and S.D.C. to BIG-UNICAMP. We are grateful to J. Molina and E.G.S. Luna for discussions.

References

1. P.A.S. Carvalho, A.F. Martini, M.J. Menon, Eur. Phys. J. C **39**, 359 (2005)
2. M.M. Block, R.N. Cahn, Rev. Mod. Phys. **57**, 563 (1985)
3. S. Eidelman et al., Phys. Lett. B **592**, 1 (2004) and 2005 partial update for the 2006 edition available on the PDG www pages (URL: http://pdg.lbl.gov)
4. E811 Collaboration, C. Avila et al., Phys. Lett. B **537**, 41 (2002)
5. K.R. Schubert, Landolt-Börnstein, Numerical Data and Functional Relationships in Science and Technology, New Series, Vol. I/9a (Springer-Verlag, Berlin, 1979)
6. R.F. Ávila, E.G.S. Luna, M.J. Menon, Phys. Rev. D **67**, 054020 (2003)
7. V. Bartenev et al., Phys. Rev. Lett. **31**, 1088 (1973); N.A. Amos et al., Nucl. Phys. B **262**, 689 (1985); A. Breakstone et al., Nucl. Phys. B **248**, 253 (1984); M. Ambrosio et al., Phys. Lett. B **115**, 495 (1982); C. Augier et al., Phys. Lett. B **316**, 448 (1993); F. Abe et al., Phys. Rev. D **50**, 5518 (1994)
8. E710 Collaboration, N.A. Amos et al., Phys. Rev. Lett. **68**, 2433 (1992)
9. COMPETE Collaboration, J.R. Cudell et al., Phys. Rev. Lett. **89**, 201801 (2002); Phys. Rev. D **65**, 074024 (2002)
10. R.J. Eden, Rev. Mod. Phys. **43**, 15 (1971)
11. S.M. Roy, Phys. Rep. **5**, 125 (1972); J. Fischer, Phys. Rep. **76**, 157 (1981); P. Valin, Phys. Rep. **203**, 233 (1991)
12. Y.S. Vernov, M.N. Mnatsakanova, Phys. Part. Nucl., **32**, 589 (2001)
13. A. Martin, Commun. Math. Phys. **219**, 191 (2001); arXiv:hep-ph/0005257; Lect. Notes Phys. **588**, 127 (2000); arXiv:hep-ph/9906393
14. M. Froissart, Phys. Rev. **123**, 1053 (1961); A. Martin, Il Nuovo Cimento A **42**, 930 (1966)
15. G. Grunberg, T.N. Truong, Phys. Rev. Lett. B **31**, 63 (1973)
16. A. Martin, F. Cheung, Analyticity Properties and Bounds on Scattering Amplitudes (Gordon and Breach Science Publishers, New York, 1970)
17. N.V. Gribov, A.A. Migdal, Yad. Fiz. **8**, 1002; Sov J. Nucl. Phys. **8**, 583 (1969); J.B. Bronzan, Argonne Symposium on the Pomeron, ANL/HEP-7327 (1973), p. 33; J.D. Jackson, 1973 Scottish Summer School, LBL-2079 (1973) p. 39; K. Kang, B. Nicolescu, Phys. Rev. D **11**, 2461 (1975)
18. J.B. Bronzan, G.L. Kane, U.P. Sukhatme, Phys. Lett. B **49**, 272 (1974)
19. R.F. Ávila, M.J. Menon, Nucl. Phys. A **744**, 249 (2004)
20. J. Fischer, P. Kolář, J. Math. Phys. **25**, 2538 (1984); Phys. Lett. B **64**, 45 (1976)
21. W. Faissler et al., Phys. Rev. D **23**, 33 (1981)
22. CDF Collaboration, F. Abe et al., Phys. Rev. D **50**, 5518 (1994)
23. V. Barger, L. Luthe, R.J.N. Phillips, Nucl. Phys. B **88**, 237 (1975)
24. W. Grein, R. Guigas, P. Kroll, Nucl. Phys. B **89**, 93 (1975)
25. P. Kroll, Fortschr. Phys. **24**, 565 (1976); Nucl. Phys. B **82**, 510 (1974)
26. E. Ferreira, F. Pereira, G.A. Perez, in IX Hadron Physics and VII Relativistic Aspects of Nuclear Physics, Angra dos Reis, 2004, ed. by M.E. Bracco et al. (AIP, New York 2004) p. 557
27. S. Mandelstam, Phys. Rev. **112**, 1344 (1958)
28. S. Mandelstam, Il Nuovo Cimento **25**, 658 (1960)
29. D. Desgrolard, M. Giffon, E. Predazzi, Z. Phys. C **63**, 241 (1994)
30. C. Bourrely, J. Soffer, T.T. Wu, Eur. Phys. J. C **28**, 97 (2003)
31. A. Donnachie, P.V. Landshoff, Z. Phys. C **2**, 55 (1979); Phys. Lett. B **123**, 345 (1983); Nucl Phys. B **267**, 690 (1986); Phys. Lett. B **296**, 227 (1992)
32. M.M. Block, E.M. Gregores, F. Halzen, G. Pancheri, Phys. Rev. D **58**, 017503 (1998); **60**, 054024 (1999)
33. L. Lukaszuk, B. Nicolescu, Lett. Nuovo Cimento **8**, 405 (1973); D. Bernard, P. Gauron, B. Nicolescu, Phys. Lett. B **199**, 125 (1987); P. Gauron, B. Nicolescu, E. Leader, Nucl. Phys. B **299**, 640 (1988)
34. CDF Collaboration, F. Abe et al., Phys. Rev. D **50**, 5550 (1994)
35. S. Bültmann et al., Phys. Lett. B **579**, 245 (2004)
36. www.fnal.gov/pub/today04-03-18.html
37. J. Molina, Doctoral Thesis, Centro Brasileiro de Pesquisas Físicas, Rio de Janeiro, Brazil (2003)
38. A. Martin, Phys. Lett. B **404**, 137 (1997)
39. M.M. Block, arXiv:physics/0506010
40. J.R. Cudell, A. Lengyel, E. Martynov, arXiv:hep-ph/0511073
41. J.R. Cudell, E. Martynov, O. Selyugin, A. Lengyel, Phys. Lett. B **587**, 189 (2004)